

**Phase transition between the CaCl<sub>2</sub>-type and  $\alpha$ -PbO<sub>2</sub>-type structures of germanium dioxide**

Shigeaki Ono

*Institute for Frontier Research on Earth Evolution, Japan Marine Science and Technology Center, 2-15 Natsushima-cho, Yokosuka-shi, Kanagawa 237-0061, Japan*

Taku Tsuchiya and Kei Hirose

*Department of Earth and Planetary Sciences, Tokyo Institute of Technology, 2-12-1 Ookayama, Meguro, Tokyo 152-8551, Japan*

Yasuo Ohishi

*Japan Synchrotron Radiation Research Institute, Mikazuki-cho, Sayo-gun, Hyogo 679-5198, Japan*

(Received 29 November 2002; revised manuscript received 12 March 2003; published 16 October 2003)

Observations of the phase transition between the CaCl<sub>2</sub>-type (*Pnmm*) and  $\alpha$ -PbO<sub>2</sub>-type (*Pbcn*) structures of germanium dioxide (GeO<sub>2</sub>) were carried out using quench and *in situ* x-ray diffraction methods in a laser-heated diamond anvil cell (LHDAC). First-principle theoretical simulations were also performed to complement the experimental results. The experiments showed that the transition had a positive  $dP/dT$  dependence. The phase boundary between the CaCl<sub>2</sub>-type and  $\alpha$ -PbO<sub>2</sub>-type structures in the temperature range 1500–2400 K was determined to be  $P$  (GPa) =  $(53 \pm 3) + (0.011 \pm 0.005)(T - 1800)$  (K) based on the equation of state of platinum and the ruby scale. The positive slope of the transition is consistent with the known phase boundary between the CaCl<sub>2</sub>-type and  $\alpha$ -PbO<sub>2</sub>-type structures of tin dioxide (SnO<sub>2</sub>) as germanium dioxide analog and theoretical simulation results. However, our results do not agree with the slope of the phase boundary of silica (SiO<sub>2</sub>), which has been reported to have a negative slope.

DOI: 10.1103/PhysRevB.68.134108

PACS number(s): 62.50.+p, 61.10.-i, 61.50.Ks

**I. INTRODUCTION**

The sequence of phase transitions in GeO<sub>2</sub> has attracted special attention because GeO<sub>2</sub> is an analog of silica (SiO<sub>2</sub>),<sup>1</sup> which is an important component of the Earth's mantle. One particular study of the high-pressure phase transitions in silica has recently attracted significant attention. The discovery of stishovite (rutile-type structure) from impact craters has led to several experimental investigations on the pressure and temperature stability relationship of these phases. It has been suggested that free silica could exist in the subducted oceanic crust in the lower mantle of the Earth.<sup>2</sup> Knowledge of the nature and mechanisms of these transitions and of the structures of post-stishovite phases are crucial for understanding the physical and seismological properties of the lower mantle. The lack of an adequate understanding of the high-pressure behavior of silica has motivated many theoretical and experimental studies on the phase transitions in silica. Theoretical calculations<sup>3,4</sup> have predicted that silica exhibits the following sequence of high-pressure phase transitions: from stishovite (rutile type), to CaCl<sub>2</sub> type,  $\alpha$ -PbO<sub>2</sub> type, and finally pyrite type. However, high-pressure experiments have failed to establish the pressure at which the transition between the CaCl<sub>2</sub> and  $\alpha$ -PbO<sub>2</sub> types of silica occurs, and there are conflicting values in the literature.<sup>5–8</sup>

Tin dioxide, SnO<sub>2</sub>, which is also analogous to silica, shows a similar sequence of phase transitions (i.e., from rutile type to CaCl<sub>2</sub> type,  $\alpha$ -PbO<sub>2</sub> type, and finally pyrite type).<sup>9,10</sup> Moreover, in GeO<sub>2</sub>, a similar series of phase transitions has also been observed and calculated.<sup>11–16</sup> Interest has therefore been focused on this analogous structure of silica. Although the phase transition from the CaCl<sub>2</sub> type to

$\alpha$ -PbO<sub>2</sub> type structure of GeO<sub>2</sub> was confirmed,<sup>15</sup> this phase boundary has not been determined. An understanding of the GeO<sub>2</sub> analog would make a valuable contribution to the understanding of the transition between the CaCl<sub>2</sub>-type and the  $\alpha$ -PbO<sub>2</sub>-type structures of silica.

We performed our experiments using a laser-heated diamond anvil cell (LHDAC), which made it possible to acquire precise data on the sample at high pressures and temperatures, and we also employed intense x rays from a synchrotron radiation source. Moreover, the quenched samples were further analyzed using Raman spectroscopy. In this report, we provide the results of our *in situ* x-ray and Raman observations on the high-pressure phases of GeO<sub>2</sub>. We also discuss the phase boundary between the CaCl<sub>2</sub> and  $\alpha$ -PbO<sub>2</sub> types of GeO<sub>2</sub>. The first-principle simulations were also performed to check and augment the observed phase relations of GeO<sub>2</sub> from the theoretical point of view.

**II. EXPERIMENT**

High-pressure x-ray diffraction experiments were performed using an LHDAC. Powdered  $\alpha$ -quartz-type GeO<sub>2</sub> (purity 99.9999%) was loaded into a 100- $\mu$ m-diameter holes drilled into rhenium gasket that was preindented to a thickness of 30–70  $\mu$ m. Platinum powder was mixed with the sample to absorb the laser radiation to provide a heat source, and the Pt was also as an internal pressure calibrant. Sodium chloride was used as the pressure medium, which minimized the pressure and temperature gradients across the sample. For the quench experiments, the samples were heated using the TEM<sub>01</sub> (donut) mode YLF laser (Fig. 1), and a multi-mode Nd:YAG laser<sup>17</sup> were used for the *in situ* x-ray experiments employing a double-sided laser heating technique that

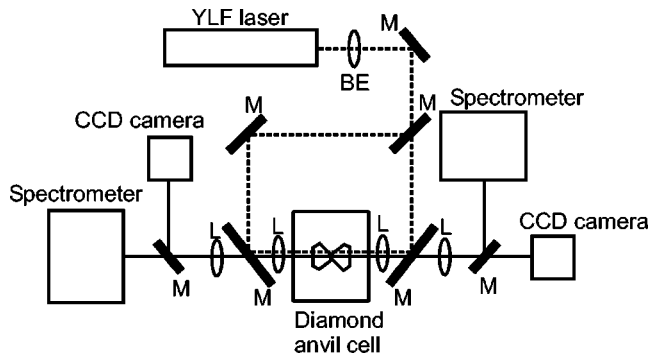


FIG. 1. Schematic diagram of the experimental design of YLF-type LHDAC. Abbreviations are lens (*L*) and mirror (*M*).

minimized the axial and radial temperature gradients across the heated area.<sup>18</sup> The heated spot diameter was about 20–30  $\mu\text{m}$  for the YLF laser, and 70–100  $\mu\text{m}$  for Nd:YAG laser. The sample temperature was measured on one side of the LHDAC using a spectroradiometric system that consisted of a thermoelectrically cooled CCD detector and a spectrograph.<sup>19</sup> The sample temperature was measured on one side of the sample using a spectroradiometric method. The spectroradiometric system consists of a thermoelectrically cooled CCD detector (Princeton Instruments, HAM 256 $\times$ 1024) and a spectrograph (Acton Research, SpectraPro-150). A grating of 300 g/mm was used, and covers the wavelength range of 460–925 nm with a central wavelength at 700 nm. The imaging spectrometer allows us to simultaneously measure all points on a linear temperature profile across a laser-heated spot. The entrance slit of the spectrograph is used to select a thin line traversing the laser spot. A temperature profile across the hotspot of about 100  $\mu\text{m}$  in 40 pixels is measured (Fig. 2). Temperatures are determined by fitting the thermal radiation spectrum between 600 and 800 nm to the Planck radiation function. The system response was calibrated by use of a tungsten ribbon lamp (OL550, Optronic Laboratories) with known radiance. The accuracy of temperature measurement using spectral radiometry in the diamond anvil cell is affected by the wavelength

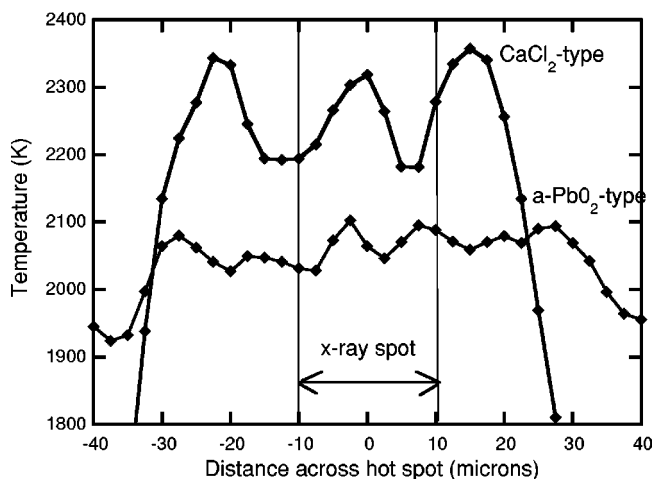


FIG. 2. A temperature profile across the hotspot heated by the laser can be obtained for each measurement.

dependence of emissivity and the systems optical aberration. However, no data of emissivity are available at high  $P$ - $T$ . Therefore, the emissivity of tungsten<sup>20</sup> is used for the radiation spectrum from the heated sample. In order to reduce the chromatic aberration effect of the optical system, it is very important to minimize temperature gradients in the laser heating spot. Therefore, our efforts in enlarging the heating spots are not only to establish a large heating volume, but also to minimize the chromatic aberration effect and so improve the accuracy of temperature measurement. The temperature error in our experiments was estimated to be within about  $\pm 150^\circ\text{C}$ .

The heated samples were probed using angle-dispersive x-ray diffraction at the BL10XU synchrotron beam line (operating at 8 GeV and 70–100 mA) of the SPring-8, a synchrotron radiation source at the Japan Synchrotron Radiation Research Institute (JASRI) in Japan. The incident x-ray beam was monochromatized to a wavelength of 0.4122  $\text{\AA}$ . The x-ray beam was collimated to diameter of 20  $\mu\text{m}$ . More detailed descriptions of the laser-heated technique using the synchrotron x ray at Spring-8 are given by Ono *et al.*<sup>19</sup> The observed intensities on the imaging plates were integrated as a function of  $2\theta$  using the FIT2D code to obtain conventional, one-dimensional diffraction profiles. The diffraction profiles were refined using the GSAS package to obtain the cell parameters and volumes for  $\text{GeO}_2$  and Pt. The pressure was determined from the observed unit cell volume of platinum from the Pt equation of state (EOS) of Holmes *et al.*,<sup>21</sup> with the electronic thermal pressure correction of Tsuchiya and Kawamura.<sup>22</sup> The uncertainty in the pressure value was related to the experimental temperature, because we used the platinum EOS. Moreover, a pressure gradient could have existed in the sample, even at high sample temperatures. Therefore, the maximum pressure error was greater than 2 GPa at high temperatures.

In the quench experiments, the pressure was determined using the ruby scale.<sup>23</sup> The pressure-dependent ruby fluorescence shift was measured after the laser heating. As the ruby scale is not applicable at high temperatures, the estimation of the pressure at high temperatures for the quench experiments included a correction for the thermal pressure. In the case of our study of *in situ* x-ray experiments, the difference between a unit cell volume of platinum during heating and that after temperature quench was small. This indicates that the pressure during heating seemed to increase by thermal pressure. However, the pressure-temperature paths in a laser heated diamond anvil cell experiments are generally complicated.<sup>24</sup> The effects of thermal pressure, release of deviatoric stress, and relaxation of the DAC itself cause the change of pressure. Therefore, the pressure error in our quench experiments was estimated to be greater than 5 GPa. After heating, the samples were investigated by using micro-Raman spectroscopy, and any phases synthesized were identified. The micro-Raman spectra were obtained using the 532 nm laser radiation line. The laser spot focus was reduced to a diameter of about 5  $\mu\text{m}$ , which was smaller than the heated spot.

The polymorphic relations of  $\text{GeO}_2$  were also investigated from the first-principle total energy calculations based on

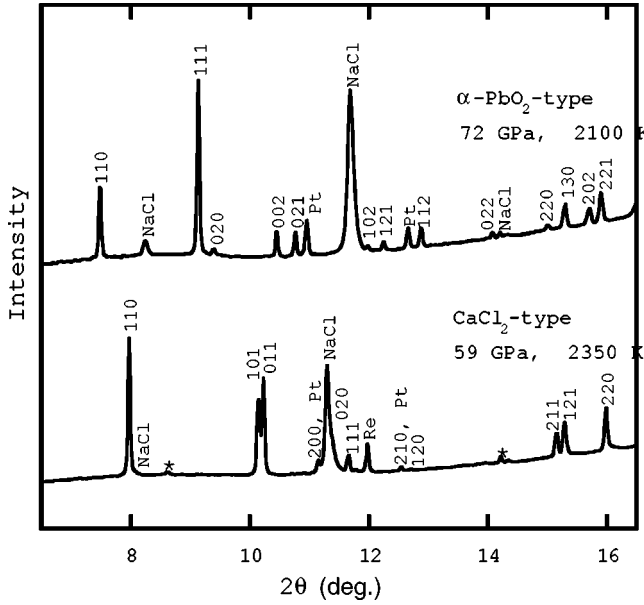


FIG. 3. X-ray diffraction pattern for  $\text{GeO}_2$  phases obtained using angle-dispersive technique with LHDAC at high  $P$ - $T$  conditions. Abbreviations of peaks are as follows: Pt, platinum as internal pressure maker; NaCl, sodium chloride as pressure medium; Re, rhenium gasket; stars, small unknown peaks.

density functional formalism.<sup>25</sup> In our study, the local density approximation approach<sup>26</sup> was adapted to use the exchange-correlation potential, and a pseudopotential with a plane-wave basis was used to solve the electronic structure. The pseudopotentials were constructed based on the Troullier-Martins-type norm-conserving scheme<sup>27</sup> with Ge and O reference configurations of  $3d^{10}4s^24p^24f^0$  and  $2s^22p^4$ , respectively. Because of the strong closed-shell interaction between the Ge  $3d$  orbitals and the O  $2s$  orbitals in  $\text{GeO}_2$ , the potential of the semicore Ge  $3d$  shell had to be included

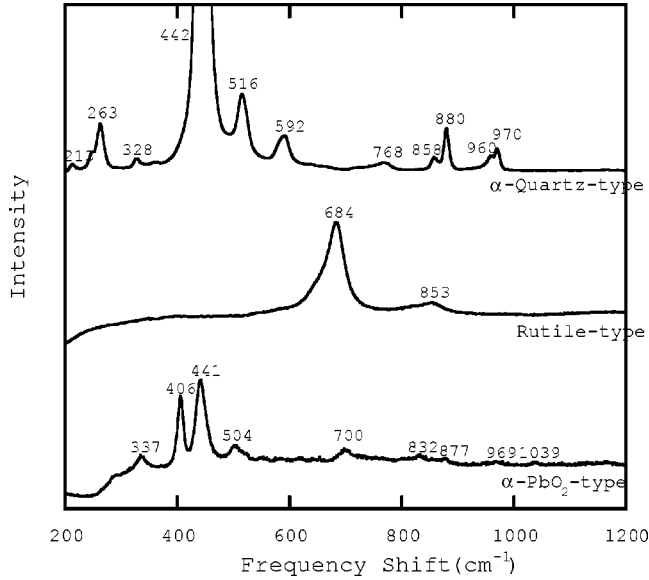
as a valence shell to represent the correct ground state. The local component of the potential was treated as an  $f$ -like form to avoid the so-called “ghost state.”<sup>28</sup> This type of pseudopotential can produce the lattice parameters in full accordance with all-electron calculations, but it is difficult. The cutoff energy of the plane-wave expansion of the wave function was set at 160 Ry.

### III. RESULTS

In the case of the *in situ* x-ray experiments, after pressurizing the starting material to the desired pressure, the temperature was increased to transform the materials to the high-pressure form. We performed diffraction measurements at the desired  $P$ - $T$  conditions. The duration of each measurement was typically 3–5 min. Figure 3 shows the acquired x-ray diffraction data. The stable phase at each  $P$ - $T$  was determined from the diffraction peaks of the  $\text{GeO}_2$  phases (Table I). In the first experiment, the  $\alpha$ - $\text{PbO}_2$ -type phase was observed at 72 GPa and 2100 K. Some diffraction lines from the internal Pt pressure calibrant and the NaCl pressure medium could be observed in addition to the diffraction lines from the sample. The quenched sample of this run was investigated using Raman spectroscopy. We observed that the  $\alpha$ -quartz-type starting material was transformed to the high-pressure phase (Fig. 3). This is consistent with our identification of the phase during *in situ* observations. In the second experiment, the  $\text{CaCl}_2$ -type phase was observed at 59 GPa and 2350 K (Table I). The  $\text{CaCl}_2$ -type phase was not recoverable on quenching, as it is converted to the rutile-type phase on releasing the pressure.<sup>12</sup> The sample quenched from 59 GPa and 2350 K exhibited the rutile-type phase from the Raman spectroscopy measurements (Fig. 4). The spectrum in Fig. 4 agrees with previous studies.<sup>29,30</sup> The  $A_{1g}$  Raman mode at  $684\text{ cm}^{-1}$  and the  $B_{2g}$  Raman mode at  $853\text{ cm}^{-1}$  were observed. Also, the  $E_g$  Raman mode was identified at

TABLE I. Observed and calculated x-ray diffraction patterns of  $\text{CaCl}_2$ -type and  $\alpha$ - $\text{PbO}_2$ -type phases. Calculated  $d$  spacings are based on orthorhombic unit cell dimensions;  $\text{CaCl}_2$ -type structure,  $a=4.240(2)\text{ \AA}$ ,  $b=4.145(2)\text{ \AA}$ ,  $c=2.786(1)$ , and  $48.97(4)\text{ \AA}^3$ ;  $\alpha$ - $\text{PbO}_2$ -type structure,  $a=4.051(1)\text{ \AA}$ ,  $b=5.028(1)\text{ \AA}$ ,  $c=4.522(1)$ , and  $92.10(4)\text{ \AA}^3$ .

$\text{CaCl}_2$	2350 K	59 GPa		$\alpha$ - $\text{PbO}_2$	2100 K	72 GPa	
$hkl$	$d_{\text{obs}}\text{ \AA}$	$d_{\text{cal}}\text{ \AA}$	$\Delta d$	$hkl$	$d_{\text{obs}}\text{ \AA}$	$d_{\text{cal}}\text{ \AA}$	$\Delta d$
110	2.9637	2.9640	-0.0003	110	3.1557	3.1546	0.0011
101	2.3295	2.3286	0.0009	111	2.5874	2.5872	0.0002
011	2.3106	2.3125	-0.0019	020	2.5166	2.5141	0.0025
200		2.1200		002	2.2619	2.2608	0.0011
020		2.0726		021	2.1964	2.1973	-0.0009
111	2.0290	2.0302	-0.0012	200		2.0255	
210		1.8875		102	1.9744	1.9742	0.0002
120	1.8616	1.8620	-0.0004	121	1.9313	1.9314	-0.0001
211	1.5628	1.5627	0.0001	112	1.8371	1.8376	-0.0005
121	1.5488	1.5481	0.0007	022	1.6815	1.6811	0.0004
220	1.4819	1.4820	-0.0001	220	1.5775	1.5773	0.0002
				130	1.5482	1.5487	-0.0005
				202	1.5081	1.5086	-0.0005
				221	1.4897	1.4893	0.0004


 FIG. 4. Observed Raman spectra of quenched  $\text{GeO}_2$  samples.

the low-frequency side of the  $A_{1g}$  mode.

In the case of the quench experiments, the Raman spectrum of the  $\alpha$ -quartz-type  $\text{GeO}_2$  starting material at ambient conditions is shown in Fig. 4. The spectrum is characterized by an extremely strong  $A_1$  mode at  $442 \text{ cm}^{-1}$ . The frequency of the  $A_1$  Raman mode increased with increasing pressure. Significant changes in the Raman spectrum began when the  $\alpha$ -quartz-type  $\text{GeO}_2$  was compressed above 7 GPa. The Raman modes of the  $\alpha$ -quartz-type  $\text{GeO}_2$  decreased strongly in intensity with increasing pressure. After pressurizing the sample above 40 GPa, no Raman mode were observed. Then, the temperature of the sample was increased using the YLF laser. The heating duration of each measurement was typically 2–5 min. After quenching, the identification of the high-pressure phase of  $\text{GeO}_2$  was based on the Raman spectroscopy results, which are summarized in Table II. The uncertainties in the pressure at high temperatures in the quench experiments were greater than those in the *in situ* x-ray experiments, because the correction using the thermal pressure had a considerable error.

The theoretical structural parameters of the predicted stable phases of  $\text{GeO}_2$  are given in Table III using available data. We obtained those data from the ground-state energy minimization of the electronic states and ionic configurations. Close agreement of the LDA results with the experimental lattice constants, which is the same degree of accuracy as the previous results of Lodziana *et al.*,<sup>13</sup> are obtained. The small differences between the two calculations are probably caused by the different of pseudopotentials used. In our study, the Ge pseudopotential intrinsically includes the semi-core  $d$  shells, whereas Lodziana *et al.*<sup>13</sup> used the partial core correction within an ultrasoft scheme. Table III also shows that GGA provides too large values of cell parameters compared to the experimental and the LDA structural properties. We found that gradient corrections increase the lattice parameters by roughly 2%.

The calculated enthalpy relations between the rutile-type,  $\text{CaCl}_2$ -type,  $\alpha$ - $\text{PbO}_2$ -type, and pyrite-type phases are demon-

 TABLE II. Experimental conditions and results in  $\text{GeO}_2$ . Abbreviations are as follows: *t*, Heating duration; A,  $\alpha$ - $\text{PbO}_2$ -type phase; C,  $\text{CaCl}_2$ -type phase.

<i>P</i> (GPa)	<i>T</i> (K)	<i>t</i> (min)	Phases
<i>In situ</i> x-ray			
71.7	2100	5	A
59.1	2370	5	C
Quench			
62.7	1750	2	A
61.4	1950	3	A
61.6	1850	3	A
52.6	1700	5	A
51.6	1700	5	C
57.1	2000	2	A
68.6	1850	2	A
68.9	1900	5	A
58.5	1850	5	A
51.8	1950	5	C
55.7	2150	5	C
65.5	2200	1	A
76.2	2050	2	A
52.3	1900	4	C
65.0	1950	5	A
70.5	1950	10	A

strated in Fig. 5. The transition pressures from rutile type to  $\text{CaCl}_2$  type, from  $\text{CaCl}_2$  type to  $\alpha$ - $\text{PbO}_2$  type, and from  $\alpha$ - $\text{PbO}_2$  type to pyrite type were found by the LDA calculation to be 19, 30, and 59 GPa, respectively, which are generally consistent with the values of 19, 36, and 65.5 GPa reported by Lodziana *et al.*<sup>13</sup> The agreement of the rutile- $\text{CaCl}_2$  transition pressure means that the transition pressures

 TABLE III. Calculated structural parameters of  $\text{GeO}_2$  polymorphs at specified pressures with previous results. *L*, Lodziana *et al.* (Ref. 13).

Phase Space group	Pressure (GPa)	Cell param. Å		<i>L</i>	Experiments
		This study LDA	GGA		
Rutile type $P4_2/mnm$	0	a=4.408	4.492	4.384	4.407 <sup>a</sup>
		c=2.887	2.923	2.864	2.862 <sup>a</sup>
$\text{CaCl}_2$ -type $Pnmm$	30	a=4.313	4.364	4.281	4.258 <sup>b</sup>
		b=4.157	4.220	4.143	4.203 <sup>b</sup>
		c=2.819	2.854	2.798	2.805 <sup>b</sup>
$\alpha\text{PbO}_2$ -type $Pbcn$	40	a=4.611	4.668	4.579	4.583 <sup>c</sup>
		b=4.124	4.172	4.096	4.111 <sup>c</sup>
		c=5.119	5.184	5.088	5.099 <sup>c</sup>
Pyrite-type $Pa\bar{3}$	70	a=4.434	4.482	4.405	4.333 <sup>d</sup>

<sup>a</sup>1 atm (Ref. 40).

<sup>b</sup>30.1 GPa (Ref. 14).

<sup>c</sup>41.1 GPa (Ref. 15).

<sup>d</sup>107.8 GPa (Ref. 15).

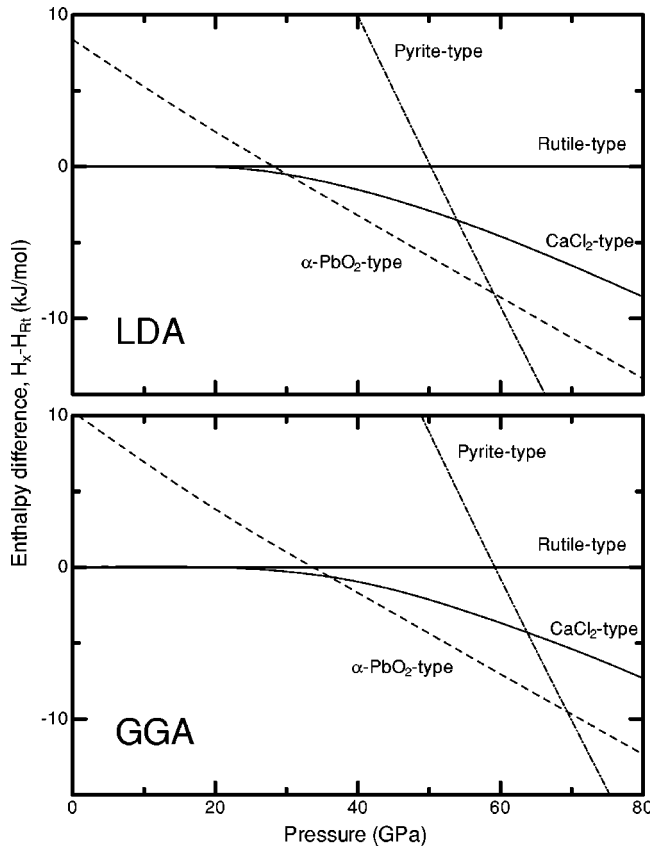


FIG. 5. Calculated enthalpy differences of respective phases from enthalpy of the rutile-type phase by LDA (upper panel) and GGA (lower panel). The solid, dashed, and dot-dashed lines represent the results of the  $\text{CaCl}_2$ -type,  $\alpha\text{-PbO}_2$ -type, and pyrite-type structures, respectively.

do not significantly depend on the method of calculation or the type of pseudopotential used. On the other hand, the transition pressures by the GGA calculation for rutile- $\text{CaCl}_2$ ,  $\text{CaCl}_2$ - $\alpha\text{-PbO}_2$  and  $\alpha\text{-PbO}_2$ -pyrite are 21, 36, and 69.5 GPa, which are higher than those by LDA. The difference is larger for the higher-pressure transition. In the case of the  $\alpha\text{-PbO}_2$ -pyrite transition, the boundary calculated by GGA is about 10 GPa higher than that by LDA. Such difference of transition pressures calculated by LDA and GGA was also found in  $\text{SiO}_2$  polymorphs.<sup>31</sup> Demuth *et al.*<sup>31</sup> reported that the transition pressures provided by GGA were more reasonable than those by LDA for low-pressure polymorphs of  $\text{SiO}_2$ , although the structural parameters are better reproduced by LDA.

The results of our determinations of  $\text{CaCl}_2$ -type and  $\alpha\text{-PbO}_2$ -type structure stability fields are summarized in Fig. 6. The transition boundary has a positive  $dP/dT$  slope. The boundary in Fig. 6 is represented by the following linear equation:

$$P(\text{GPa}) = (53 \pm 3) + (0.011 \pm 0.005) \times (T - 1800)(\text{K}).$$

The theoretical zero-temperature value of  $\text{CaCl}_2$ -type to  $\alpha\text{-PbO}_2$ -type structure transition pressures of  $\text{GeO}_2$  is 30.5 GPa (LDA) and 36 GPa (GGA). Our experimental results determined the transition pressure to be 33 GPa at 0 K, which is in close agreement with the *ab initio* study.

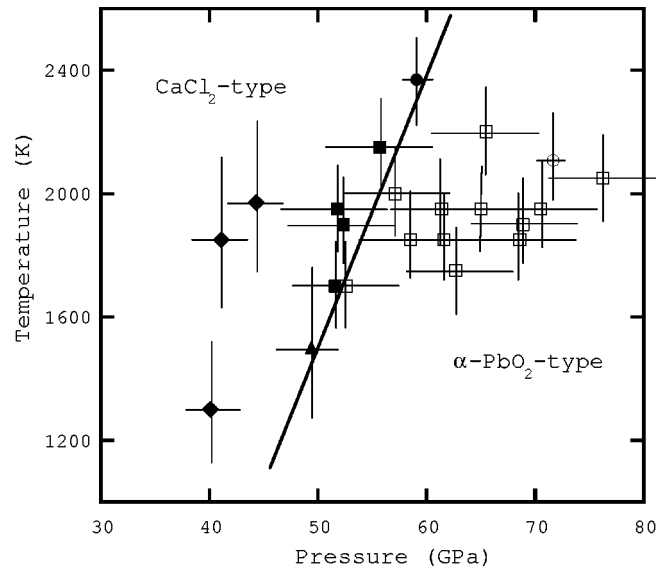


FIG. 6. Experimental results and a phase boundary determined by both in situ and quench experiments. Abbreviations are as follows: solid circle,  $\text{CaCl}_2$ -type phase of *in situ* x-ray experiments; open circles,  $\alpha\text{-PbO}_2$ -type phases of *in situ* x-ray experiments; solid squares,  $\text{CaCl}_2$ -type phase of the quench experiments; open squares,  $\alpha\text{-PbO}_2$ -type phases of the quench experiments; solid triangle, a mixture of two phases (Ref. 15); solid diamonds,  $\text{CaCl}_2$ -type phase (Ref. 14).

#### IV. DISCUSSION AND CONCLUSIONS

Figure 7 shows the phase diagram of  $\text{GeO}_2$  determined by our results and from previous studies. At ambient pressure, rutile-type and  $\alpha$ -quartz-type phases are stable at low and high temperatures, respectively. Then, the rutile-type phase transforms to the  $\text{CaCl}_2$ -type phase with increasing pressure, which is indicative of a second-order phase transition. This phase boundary has a positive  $dP/dT$  slope.<sup>14</sup> We found that the transformation from the  $\text{CaCl}_2$ -type phase to the

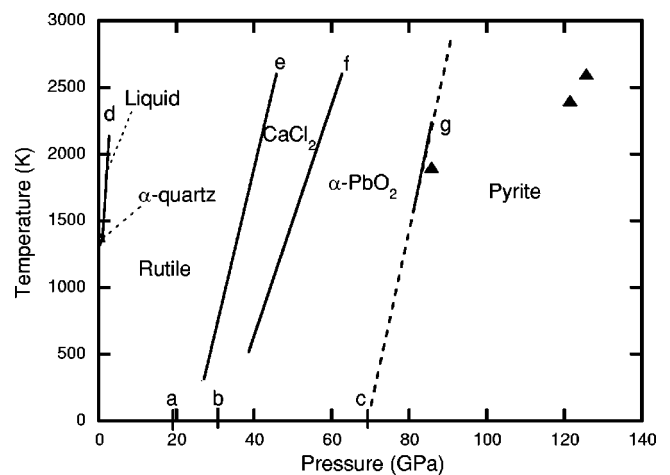


FIG. 7. Phase diagram of  $\text{GeO}_2$ . Solid triangles are pyrite-type phase reported by Ono *et al.* (Ref. 15). Abbreviations are as follows: a, b, and c, calculated transition points at 0 K using the GGA method in this study; d, Liu and Bassett (Ref. 39); e, Ono *et al.* (Ref. 14); f, this study; g, estimated phase boundary.

TABLE IV. The  $dP/dT$  slope of phase boundary between the  $\text{CaCl}_2$ -type and  $\alpha\text{-PbO}_2$ -type structures in the  $\text{AO}_2$  phase. A, Dubrovinsky *et al.* (Ref. 7); B, this study; C, Suito *et al.* (Ref. 33).

	$dP/dT$ (MPa/K)	References
$\text{SiO}_2$	-11	A
$\text{GeO}_2$	11	B
$\text{SnO}_2$	2.2	C

$\alpha\text{-PbO}_2$ -type phase, also had a positive  $dP/dT$  slope. At higher pressures, the transition from the  $\alpha\text{-PbO}_2$ -type phase to the pyrite-type phase has been reported.<sup>15</sup> The slope of the  $dP/dT$  transition is difficult to determine, but this transition seems to have a positive  $dP/dT$  slope if we assume that the phase boundary at 0 K is located at either the theoretical pressure of 59 GPa (LDA) and 69.5 GPa (GGA) in this study or the 65.5 GPa of Lodziana *et al.*<sup>13</sup> Consequently,  $\text{GeO}_2$  shows the following sequence of phase transitions: rutile type,  $\text{CaCl}_2$  type,  $\alpha\text{-PbO}_2$  type, and finally, pyrite type, and all the transitions have a positive  $dP/dT$  slope.

The transition sequence in  $\text{GeO}_2$  is the same as that in  $\text{SnO}_2$  reported in previous studies.<sup>9,10</sup> Furthermore, the experimental studies reported that the silica,  $\text{SiO}_2$ , showed this same transition sequence, except for the pyrite-type phase.<sup>5,6,8,32</sup> The low-pressure limit of the stability field of the pyrite-type phase in  $\text{SiO}_2$  seems to be too high to synthesize this form by experiment.<sup>3,4</sup> From the results of the  $\text{SiO}_2$  and  $\text{SnO}_2$  analog of  $\text{GeO}_2$ , the high-pressure transition sequence of  $\text{GeO}_2$  from rutile type to  $\text{CaCl}_2$  type to  $\alpha\text{-PbO}_2$  type to pyrite type seems reasonable.

Table IV shows a comparison of the  $dP/dT$  slopes of the phase boundary between the  $\text{CaCl}_2$ -type and  $\alpha\text{-PbO}_2$ -type structures in  $\text{SiO}_2$ ,  $\text{GeO}_2$ , and  $\text{SnO}_2$ . Our results for  $\text{GeO}_2$  show a positive slope, which agrees with that of  $\text{SnO}_2$ .<sup>33</sup> However, a negative slope for  $\text{SiO}_2$  was reported by Dubrovinsky *et al.*<sup>7</sup> At the lower phase transition between the rutile-type and  $\text{CaCl}_2$ -type structures, positive  $dP/dT$  slopes were reported for  $\text{SiO}_2$  and  $\text{GeO}_2$ .<sup>8,14</sup> Since the structural changes are similar in those phase transitions, it is difficult to

understand why  $\text{SiO}_2$  shows an exception in the transition between the  $\text{CaCl}_2$ -type and  $\alpha\text{-PbO}_2$ -type phases. Therefore, there is a need for further investigation into the  $dP/dT$  slope of the  $\text{SiO}_2$  phase boundary.

Based on relatively poor x-ray data recorded using a conventional source, previous studies have reported an  $\text{Fe}_2\text{N}$ -type structure in  $\text{GeO}_2$  at pressures above 25 GPa.<sup>34,35</sup> Recent studies using synchrotron x-ray diffraction<sup>15</sup> to pressures up to 130 GPa have confirmed that the  $\text{Fe}_2\text{N}$ -type structure reported by previous studies was in fact the  $\alpha\text{-PbO}_2$ -type structure.<sup>36</sup> Moreover, a neutron and synchrotron study has reported that  $\zeta\text{-Fe}_2\text{N}$  can exhibit the  $\alpha\text{-PbO}_2$ -type structure.<sup>37</sup>

An unknown orthorhombic structure in  $\text{GeO}_2$  has been reported at pressures above 25 GPa.<sup>38</sup> However, this phase was not observed in our experiments. This discrepancy seems to be a result of the kinetics of the phase transitions. At low temperatures, materials are often compressed in a metastable state relative to their phase boundaries, because of the small thermal energy of the atoms compared to the activation barrier for the transition. To avoid the formation of metastable phases, we used the laser-heated technique to increase the temperature to above 2000 K, and additionally to release any stress in the sample. Our heating technique seemed to enhance the phase transition. Although the high  $P$ - $T$  phase was observed after the temperature quench in the previous study, their heating temperature was lower than ours, because of technical problems they experienced. We used the method of in situ observations at the high  $P$ - $T$  conditions by using intense x rays from synchrotron radiation source. Therefore, the previously reported unknown orthorhombic phases seem to be thermally metastable.

#### ACKNOWLEDGMENTS

We thank M. Isshiki, T. Watanuki, S. Nakashima, E. Takahashi, T. Iiduka, T. Hirata, and Y. Tatsumi for help with this study. The synchrotron radiation experiments were performed at the SPring-8 with the approval of the Japan Synchrotron Radiation Research Institute (JASRI) (Proposal No. 2002A0106-ND2-np).

<sup>1</sup>J.M. Leger and J. Haines, *Eur. J. Solid State Inorg. Chem.* **34**, 785 (1997).

<sup>2</sup>S. Ono, E. Ito, and T. Katsura, *Earth Planet. Sci. Lett.* **190**, 57 (2001).

<sup>3</sup>B.B. Karki, M.C. Warren, L. Stixrude, G.J. Ackland, and J. Crain, *Phys. Rev. B* **55**, 3465 (1997).

<sup>4</sup>D.M. Teter, R.J. Hemley, G. Kresse, and J. Hafner, *Phys. Rev. Lett.* **80**, 2145 (1998).

<sup>5</sup>D. Andrault, G. Fiquet, F. Guyot, and M. Hanfland, *Science* **282**, 720 (1998).

<sup>6</sup>L.S. Dubrovinsky, S.K. Saxena, P. Lazor, R. Ahuja, O. Eriksson, J.M. Wills, and B. Johansson, *Nature (London)* **388**, 362 (1997).

<sup>7</sup>L.S. Dubrovinsky, N.A. Dubrovinskaia, S.K. Saxena, F. Tutti, S. Rekhi, T. Le Bihan, G. Shen, and J. Hu, *Chem. Phys. Lett.* **333**,

264 (2001).

<sup>8</sup>S. Ono, K. Hirose, M. Murakami, and M. Isshiki, *Earth Planet. Sci. Lett.* **197**, 187 (2002).

<sup>9</sup>J. Haines and J.M. Léger, *Phys. Rev. B* **55**, 11 144 (1997).

<sup>10</sup>S. Ono, E. Ito, T. Katsura, A. Yoneda, M. Walter, S. Urakawa, W. Utsumi, and K. Funakoshi, *Phys. Chem. Miner.* **27**, 618 (2000).

<sup>11</sup>J. Haines, J.M. Léger, C. Chateau, R. Bini, and L. Ulivi, *Phys. Rev. B* **58**, R2909 (1998).

<sup>12</sup>J. Haines, J.M. Leger, C. Chateau, and A.S. Pereira, *Phys. Chem. Miner.* **27**, 575 (2000).

<sup>13</sup>Z. Lodziana, K. Parlinski, and J. Hafner, *Phys. Rev. B* **63**, 134106 (2001).

<sup>14</sup>S. Ono, K. Hirose, N. Nishiyama, and M. Isshiki, *Am. Mineral.* **87**, 99 (2002).

- <sup>15</sup>S. Ono, K. Hirose, T. Tsuchiya, and Y. Ohishi, *Phys. Rev. B* **68**, 014103 (2003).
- <sup>16</sup>T. Tsuchiya, T. Yamanaka, and M. Matsui, *Phys. Chem. Miner.* **25**, 94 (1998).
- <sup>17</sup>S. Ono, K. Hirose, M. Isshiki, K. Mibe, and Y. Saito, *Phys. Chem. Miner.* **29**, 527 (2002).
- <sup>18</sup>G. Shen, M.L. Rivers, Y. Wang, and R. Sutton, *Rev. Sci. Instrum.* **72**, 1273 (2001).
- <sup>19</sup>S. Ono, Y. Ohishi, K. Hirose, and T. Watanuki, *J. Geophys. Res.* (to be published).
- <sup>20</sup>J.C. De Vos, *Physica (Amsterdam)* **20**, 690 (1954).
- <sup>21</sup>N.C. Holmes, J.A. Moriarty, G.R. Gathers, and W.J. Nellis, *J. Appl. Phys.* **66**, 2962 (1989).
- <sup>22</sup>T. Tsuchiya and K. Kawamura, *Phys. Rev. B* **66**, 094115 (2002).
- <sup>23</sup>H.K. Mao, J. Xu, and P.M. Bell, *J. Geophys. Res.* **91**, 4673 (1986).
- <sup>24</sup>A. Kavner and T.S. Duffy, *J. Appl. Phys.* **89**, 1907 (2001).
- <sup>25</sup>P. Hohenberg and W. Kohn, *Phys. Rev.* **136**, B864 (1964).
- <sup>26</sup>W. Kohn and L.J. Sham, *Phys. Rev.* **140**, A1133 (1965).
- <sup>27</sup>N. Troullier and J.L. Martins, *Phys. Rev. B* **43**, 1993 (1991).
- <sup>28</sup>M. Fuchs, J.L.F. Da Silva, C. Stampfl, J. Neugebauer, and M. Scheffler, *Phys. Rev. B* **65**, 245212 (2002).
- <sup>29</sup>P. Gillet, A. Le Cleac'h, and M. Madon, *J. Geophys. Res.* **95**, 21 635 (1990).
- <sup>30</sup>J.F. Scott, *Phys. Rev. B* **1**, 3488 (1970).
- <sup>31</sup>T. Demuth, Y. Jeanvoine, J. Hafner, and J.G. Angyan, *J. Phys.: Condens. Matter* **11**, 3833 (1999).
- <sup>32</sup>K.J. Kingma, R.E. Cohen, R.J. Hemley, and H.K. Mao, *Nature (London)* **374**, 243 (1995).
- <sup>33</sup>K. Suito, N. Kawai, and Y. Masuda, *Mater. Res. Bull.* **10**, 677 (1975).
- <sup>34</sup>J. Haines, J.M. Leger, and C. Chateau, *Phys. Rev. B* **61**, 8701 (2000).
- <sup>35</sup>L. Liu, W.A. Bassett, and J. Sharry, *J. Geophys. Res.* **83**, 2301 (1978).
- <sup>36</sup>K. Shiraki, T. Tsuchiya, and S. Ono, *Acta. Crystallogr.* (to be published).
- <sup>37</sup>D. Rechenbach and H. Jacobs, *J. Alloys Compd.* **235**, 15 (1996).
- <sup>38</sup>L.C. Ming and M.H. Manghnani, *Phys. Earth Planet. Inter.* **33**, 26 (1983).
- <sup>39</sup>L. Liu and W.A. Bassett, *Elements, Oxides, Silicates* (Oxford University Press, New York, 1986), p. 113.
- <sup>40</sup>A.A. Bolzan, C. Fong, B. Kennedy, and C. Howard, *Acta Crystallogr., Sect. B: Struct. Sci.* **53**, 373 (1997).